Lightweight hybrid electrical vehicle structural topology optimisation investigation focusing on crashworthiness

Christensen, J. , Bastien, C. , Blundell, M.V. , Gittens, A. and Tomlin, O.

J. Christensen et al. 2011. *Int. J. Vehicle Structures & Systems*, 3(2), 113-122
ISSN: 0975-3060 (Print), 0975-3540 (Online)
doi: 10.4273/ijvss.3.2.06

International Journal of
Vehicle Structures & Systems
Available online at www.ijvss.maftree.org

Lightweight Hybrid Electrical Vehicle Structural Topology Optimisation Investigation Focusing on Crashworthiness

Jesper Christensen[a,d], Christophe Bastien[a,b], Mike Blundell[a,c], Andrew Gittens[e,f], and Oliver Tomlin[e,g]

[a]*Faculty of Engineering and Computing,Coventry University, UK.*
[b]*Email: aa3425@coventry.ac.uk*
[c]*Email: cex403@coventry.ac.uk*
[d]*Corresponding Author, Email: aa8867@coventry.ac.uk*

[e]*Safety Development,MIRA Limited, UK.*
[f]*Email: andrew.gittens@mira.co.uk*
[g]*Email: oliver.tomlin@mira.co.uk*

ABSTRACT:

As focus on the world climate rises, so does the demand for ever more environmentally friendly technologies. The response from the automotive industry includes vehicles whose primary propulsion systems are not based upon fossil fuels. On this basis a Low Carbon Vehicle Technology Project, partly funded by the European Regional Development Fund, is currently under way; part of this project involves designing a lightweight Body In White (BIW). This has been specifically tailored to suit the drive train and general packaging requirements associated with a Hybrid Electric Vehicle (HEV). The future opportunities for new lightweight vehicle architecture have been investigated using a technique entitled topology optimisation, which extracts the idealised load paths for a given loading. The topology optimisation includes equivalent NCAP dynamic impact loading conditions, as well as torsional rigidity performance. Initially a total of 7 loading scenarios are applied on a structure comprising of various battery and range extender layouts. Two different optimisation modelling techniques have been undertaken comparing conventional boundary conditions against inertia relief, as well as studying the sensitivity of the BIW topology against the influence of load case direction and battery box stiffness. Optimal locations for the two components having the highest mass, i.e. a single battery pack and a combined range extender and fuel tank have been studied focusing upon the effects of the location of their Centre of Mass. It has been assumed that advances in battery technology will reduce the external dimensions of the battery package, thereby enabling an increased number of possible locations within the BIW.

KEYWORDS:

Body In White (BIW); Topology optimisation; Inertia Relief; Lightweight Hybrid Electric Vehicle (HEV); NCAP;

CITATION:

J. Christensen, C. Bastien, M. Blundell, A. Gittens, and O. Tomlin. 2011. Lightweight hybrid electrical vehicle structural topology optimisation investigation focusing on crashworthiness, *Int. J. Vehicle Structures & Systems*, 3(2), 113-122. doi:10.4273/ijvss.3.2.06

ACRONYMS AND NOMENCLATURE:

BIW	*Body In White*
BC	*Boundary Condition*
C_{mass}	*Component mass*
CBC	*Conventional Boundary Conditions*
CM	*Centre of Mass*
CPU	*Central Processing Unit*
cst	*Constant used for calculation, variable value*
DOF	*Degree(s) Of Freedom*
E	*Young's modulus*
{F}	*Force (column) vector*
F_{ie}	*Force originating from Inertial Effects*
FIMV	*Final Iteration Mass Value*
FT	*Fuel Tank*
g	*Gravitational acceleration (9.82 m/s^2)*
HEV	*Hybrid Electric Vehicle*
ICE	*Internal Combustion Engine*
IR	*Inertia Relief (boundary condition)*
[k]	*Stiffness matrix*
LCED	*LoCked Element Densities*
v	*Poisson's ratio*
ODB	*Offset Deformable Barrier*
p	*Penalisation factor*
ρ	*Volumetric mass density kg/m^3*
RE	*Range Extender*
{u}	*Displacement (column) vector*
ZIMV	*Zeroth Iteration Mass Value*

1. Introduction

This paper details the topology optimisation process of a BIW intended for a HEV, exposed to loading representative of legislative crash scenarios. The objective of the topology optimisation is to reduce the BIW mass by varying the location of specific HEV components. The seating arrangement of the vehicle will be 5 + 2 with the maximum length of the vehicle being less than 3900 mm. The singular propulsion system of

the vehicle will be electric. This requires that an electric motor will convert electric energy, originating from a battery pack, into mechanical motion to drive the wheels. The vehicle will be front wheel driven only. In addition, to the battery pack a RE, i.e. a small displacement ICE, combined with a Fuel Tank (FT) was added in order to expand the operating range of the vehicle. The purpose of this addition is solely to charge the battery pack. The above description clearly indicates that the setup of the vehicle in question differs significantly from the majority of "conventional" fossil fuelled vehicles currently being sold.

The intention was therefore to thoroughly investigate the possibilities of reducing the BIW mass, while accommodating the above requirements. The starting point was essentially a blank canvas, where the design volume for the topology optimisation was defined with simple limitations relating to the interior cabin space and other packaging requirements. This design volume is illustrated in Fig. 1. The approximate maximum exterior dimensions of the design volume were: (x, y, z) 3865 mm x 1850 mm x 1530 mm.

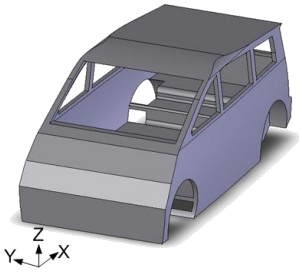

Fig. 1: Design volume

1.1. Discretisation

The above illustrated design volume was meshed using solid tetra elements with linear displacement functions and an average element size of 25.0 mm. This leads to the generation of approximately 103000 nodes and 527000 elements.

1.2. Load cases

The load cases utilised in the optimisation process were intended to be representative of the worst case legislative and NCAP dynamic impact loading scenarios. Therefore a total of seven loading scenarios were defined, these are listed below:

1. Front impact, ODB.
2. Pole impact.
3. Side barrier impact.
4. Roof crush: A-pillar.
5. Low speed centred rear impact.
6. High speed rear impact.
7. Torsion.

The approximate locations of the above defined loading scenarios (excluding number 7) are illustrated in Fig. 2.

1.3. Battery pack, range extender and fuel tank

Due to the nature of the optimisation, the loading scenarios must also incorporate the masses and associated inertial effects originating from the battery pack, the range extender and the fuel tank, in addition to the external forces illustrated in Fig. 2. Only these components have been selected for this initial study; as the individual masses of these are the highest of all key components.

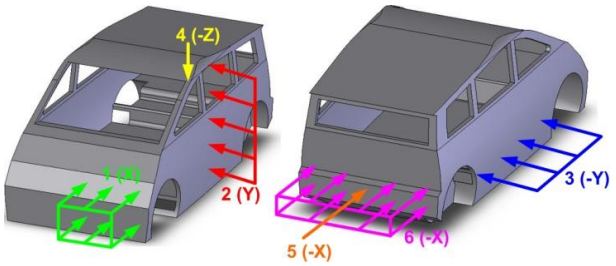

Fig. 2: Loading scenarios

Based upon present day battery technology, and the performance requirements of the battery in mind, the number of feasible locations of the battery pack within the BIW was limited. This is due to the external dimensions of the battery pack, i.e. volume. However, it was assumed that advances in battery technology in the near future will enable additional locations of the battery pack within the BIW due to reduced volume requirements. Therefore it was chosen to initially focus upon the location of the CM for the battery pack and the combined CM for the range extender and fuel tank, i.e. two CM. In order not to destabilise the topology optimisation the CM has been evenly distributed over 250 mm by 250 mm areas (in the x-y plane defined in Fig. 1). The defined masses for the two components are:

- Battery pack: 150 kg
- Range extender / fuel tank: 110 kg

The methodology used to incorporate the above defined masses within the previously defined load cases is partially dependent upon the chosen boundary conditions which will be further discussed in Section 2.

1.4. Material

The material model used for the topology optimisation is linear elastic, utilising the material characteristics of a mild grade steel:

- Young's modulus, E: 210 GPa.
- Poisson's ratio, ν: 0.3.
- Volumetric mass density, ρ: 7850 kg / m^3.

At a later stage in the design process it will become necessary to define the dynamic (non-linear and plastic) properties of the material [1], [2].

1.5. Topology optimisation methodology

The objective of the topology optimisation procedure was to minimise the volume (mass) of the design volume, as illustrated in Fig. 1. The constraints of the topology optimisation have been specified by defining maximum displacement values of relevant nodes for the individual load cases illustrated in Fig. 2. The ideal topology optimisation procedure would entail obtaining the outline of the complete BIW topology from a single model, i.e. a single optimisation run.

However, results from initial models revealed that this was not feasible. This was due to various factors, relating to e.g. load magnitude, load application areas and BC limitations. Therefore it has been necessary to "lock" the relative element densities of specific elements in order to stabilise the models, i.e. excluding these from the design volume. For more information, please see [2].

These elements are referred to as having LCED. By varying these between otherwise identical models the BIW topology can be "constructed" by interpreting the results of multiple models (optimisation runs). With the initial model setup complete, the next chapter will focus upon different BC modelling techniques.

2. Methods

As previously mentioned, two different modelling techniques, CBC and IR, have been applied to the optimisation procedure.

2.1. Conventional Boundary Conditions (CBC)

The usage of CBC requires definition of the allowable translational and rotational movements of specified nodes, i.e. constraining certain DOF of these. In other words, when solving Eqn. (1):

$$\{F\} = [k] \cdot \{u\} \tag{1}$$

The stiffness matrix[k] contains predefined values representative of the specified BC's. The applied BC's are thus utilised when Eqn. (1) is solved (directly) by multiplication of the inverted [k] matrix, i.e. implicit FE. This means that for multiple load cases (with different BC's) the stiffness matrix [k] must be reconstructed, and subsequently inverted, which can be very costly with respect to CPU time, during the optimisation process. By utilising CBC the inertial effects originating from the mass of the battery pack and the combined mass of the range extender / fuel tank have been calculated as specified in Eqn. (2):

$$F_{ie} = cst \cdot g \cdot C_{mass} \tag{2}$$

Where F_{ie} is the force (originating from inertial effects), g is the gravitational acceleration, C_{mass} is the components mass, and cst is a constant used to scale the acceleration, in order to adapt it to the individual load case. The individual values of the constant (cst) are listed below.

- 30 for load cases 1 and 6 (high speed impacts)
- 15 for load cases 2 and 3(side and barrier)
- 10 for load case 5 (low speed rear impact)
- 0 for load cases 4 and 7 (roof crush / torsion)

2.2. Inertia Relief (IR)

The following information relating to inertia relief is primarily based upon Barnett & Widrick [4]. Inertia relief utilises a significantly different approach to obtaining load equilibrium of the models in question. In this approach no DOF of any nodes are constrained (due to BC's). Instead, inertia relief works by balancing the external loading with inertial loads and accelerations within the structure itself. This is specifically done by "adding" an extra displacement-dependent load to the load vector: {F} in Eqn. (1). This implies that if two "identical" models (where one utilises CBC's and the other utilises IR) are to be solved, then theoretically the inertia relief model should be slower to compute, simply because the stiffness matrix [k] will contain additional terms. This is provided that the models in question only include a single load case and only one set of CBC's, or multiple load cases utilising one set of CBC's. The additional terms of the stiffness matrix can be appreciated by observing Eqn. (3).

$$\{F\} = [k_{IR}] \cdot \{u\} = \begin{bmatrix} [k] & 0 \\ 0 & [k_{add}] \end{bmatrix} \cdot \{u\} \tag{3}$$

Where $[k_{IR}]$ is the stiffness matrix of the IR model, [k] is the "original" stiffness matrix, i.e. the one listed in Eqn. (1), and $[k_{add}]$ represents the additional terms in the stiffness matrix, caused by the usage of IR. Thus by comparing Eqn. (1) to Eqn. (3), the fundamental difference between the CBC models and the IR models can be appreciated. The comparison indicates the existence of possibilities to(drastically) reduce the computation time of the topology optimisation, by utilising IR compared to using CBC's, if models containing multiple load cases (with different CBC's) are to be analysed. This is because the model utilising CBC's will be required to construct and invert the stiffness matrix [k] for every load case due to a change in BC's. However, the model utilising IR will be required to construct and invert $[k_{IR}]$ only once, because the BC's do not affect it.

When computing the displacements due to the individual load cases the only parameter that will have to be adapted is the load vector {F}. For the purpose of determining the stress distribution (or displacements) in connection with conducting a topology optimisation, the stresses originating from the individual load cases can simply be obtained by the method of superposition. The latter is of course only valid as long as the analysis is linear. Based upon the basic methodology of IR, it was not necessary to "transform" the inertial effects originating from the individual components, as is defined for the CBC models in Eqn. (2). Therefore the representation of these masses was simply accomplished by means of nodal masses in the vicinity of the intended CM, as described in Section 1.5.

2.3. Comparison of CBC and IR

The two previous Sections outline some of the possible differences with respect to CPU time when subsequently solving the FEM models (optimisation). As the impending optimisation was to be performed linear statically, the relationship between the stiffness matrix [k] or $[k_{IR}]$ and the volumetric mass density (ρ) was defined by the "power law for representation of elasticity properties" as Eqns. (4) and [5]:

$$\underline{[k]}(\rho) = \rho^{p}[k] \tag{4}$$

Where $\underline{[k]}$ is the penalized stiffness matrix, and p is the penalisation factor, which is used to determine the "type" of relationship between [k] and ρ. As long as *p* is equal to 1.0 the two are directly proportional (see Fig. 3).

The trial runs were conducted on 2 CPU's. A total of 74 models utilising CBC's and 73 models using IR were completed, the reasoning for the additional CBC model will be explained in the next chapter. The average CPU times are listed below:

- CBC: 59249.3 seconds (16.5 hours)
- IR: 5163.5 seconds (1.4 hours)

The above clearly indicated the significant differences in CPU time, as the usage of IR as opposed to CBC

represented a reduction in CPU time of approximately 91%. The advantage of utilising IR from a CPU point of view was obvious, but understanding the influences was key. These influences are discussed in the next Section.

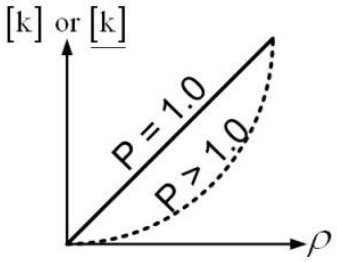

Fig. 3: Relationship between [k] and ρ

3. Application to Topology Optimisation

The previous Section discussed the effects of utilising CBC and IR with respect to the overall CPU time. This chapter will aim to discuss the model differences and related topology results.

3.1. Introduction

The main purpose of the topology optimisation was to investigate the influence of the location of the aforementioned battery box and combined range extender / fuel tank with respect to minimising the BIW mass. Therefore a series of models, where the CM of the battery pack and range extender / fuel tank was the variable were developed. These models have subsequently been solved using CBC and IR while subjected to the load cases described in Section 1.2. Fig. 4 illustrates how the areas of the design volume were discretised to define model specific locations of the CM within the BIW.

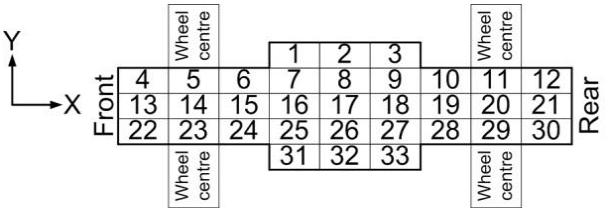

Fig. 4: Locations within BIW

The usage of two CM (i.e. battery pack and combined range extender / fuel tank) united with the discretisation illustrated in Fig. 4 led to a possible 1089 iterations (i.e. different models). In addition, if the CBC and IR aspect was considered a total of 2178 models would have to be investigated, which was not practical. Therefore a series of considerations were used to reduce the number of models. The first of such was the requirement for a symmetric BIW with respect to the xz-plane (Fig. 1) i.e. the x-axis in Fig. 4. Due to the mass difference between the battery pack (150 kg) and the range extender / fuel tank (110 kg) a similar constraint could not be applied parallel to the yz-plane in (Fig. 1) i.e. the y-axis in Fig. 4. In addition a series of considerations relating to e.g. general mass distribution eliminated additional unfeasible setups. A clear example of such a setup would be the CM of the battery pack in location 1 (Fig. 4) and the CM of the range extender / fuel tank in location 2 (Fig. 4). Thereby the number of models were reduced to 73 (per type of BC), including a model containing only a single CM for all components located in position 14 (Fig. 4) with a mass of 260 kg, this was denoted as model 68.

Two models (per BC type) intended to be used to assess the influence of the size of the battery were also implemented. In Section 2.1 it was defined how the inertial effects originating from the mass of the components in question were implemented into the models. Eqn. (2) defines how these specific forces were calculated. The set up of model 69 is illustrated in Fig. 5, where the respective locations of the battery pack as well as the range extender /fuel tank CM are indicated.

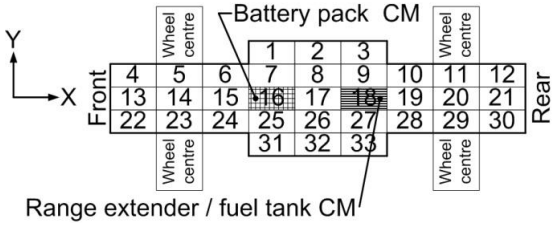

Fig. 5: Model 69

Model 69, as illustrated in Fig. 5, was subsequently copied in order to form the basis of models 71, 72 and 73. All of these were based upon the CM layout of model 69 (Fig. 5), and contained the adjustments as stated in Table 1. The setups defined in Table 1 applied to both the CBC and IR models, and were included in the 73 (times 2) aforementioned models. It was previously mentioned that a 74th model only using CBC was created. This model was also a copy of model 69, with respect to location of CM of the battery back and the CM of the combined range extender / fuel tank. The only difference between model 69 and model 74 for CBC was that an additional load case representing static deflection was added. This model thereby contained a total of 8 load cases. It made no sense to do this for the "corresponding" IR model, because the mass was directly used as an input. The reason for using this 74th model will be elaborated in the following Section. With the above definitions in place, the next Section will focus upon discussing the topology optimisation results.

Table 1: Model definitions

Model #	Adjustment from model 69 (Fig. 5)
71	2D shear panel included as roof, element thickness = 0.7 mm
72	Neither component mass nor loading (originating there from) included.
73	C_{mass} scaled by a factor of 2

3.2. Effects of component locations

For the purpose of this discussion, the design volume will be divided into "areas", as illustrated by Fig. 6. Throughout the variation of the individual models, where the main parameter was location of the CM, a general tendency of the roof topology was found. This tendency was applicable to both the CBC and the IR models. Thereby indicating that the location of the CM had only minor influence upon the topology of the roof area. This general tendency is illustrated in Fig. 7.

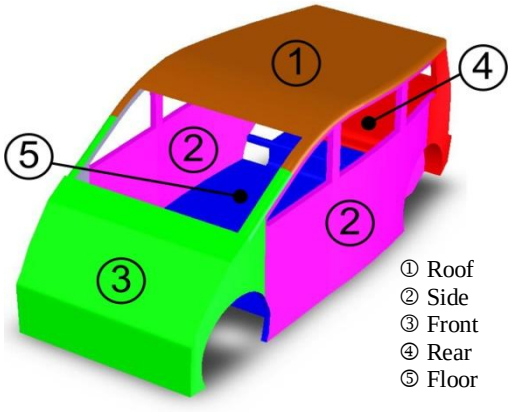

Fig. 6: Design volume areas

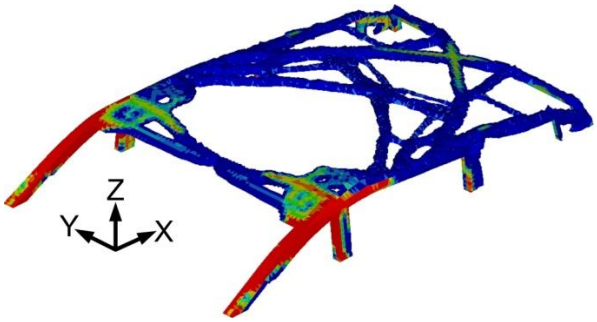

Fig. 7: Roof topology

An important factor to note when viewing Fig. 7 is the wide spread triangulation of the roof structure, which diverges significantly from conventional roof bow structures often found in modern day vehicles. The general topology illustrated in the figure is also recognised in the results of model 71, which represents the inclusion of a 2D shear panel, as defined in Section 3.1. Based on the study it was found that a clearly defined topology for the side area proved difficult to obtain. This was primarily thought to be linked with the necessity to use LCED, as discussed in Section 1.1. However, general tendencies were still found, even though some models did not display a clearly defined topology in this area. A typical example of a vaguely defined topology of the side area is illustrated in Fig. 8.

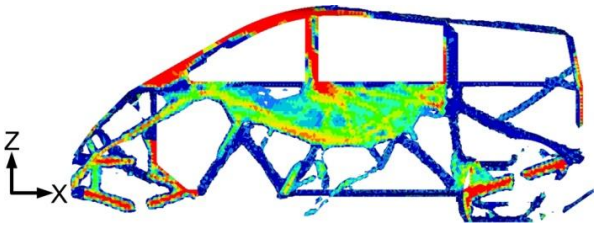

Fig. 8: Side topology

By observing Fig. 8 and the associated stress plots / distributions it is evident that additional definition of the topology in this area is desirable. A possible way of overcoming this problem is simply to adjust the penalisation factor p, as discussed in Section 2.2, and subsequently re-run the optimisation. If the desired level of definition is still not achieved supplementary models are likely to be required, which might involve adopting a different approach altogether, such as discussed in [6]. However, a general tendency for the topology of the side area throughout this study existed, indicating that the topology of this area was neither heavily influenced by the location of the components in question, nor the usage of CBC vs. IR. In line with the previously discussed areas the front did not show tendencies of significant topological difference between the CBC and IR models. In addition, the location of the CM also showed only minor local changes in topology of the individual models. Thus a general tendency for the topology of the front area representing both the CBC and the IR models could be identified. This general tendency is illustrated in Fig. 9.

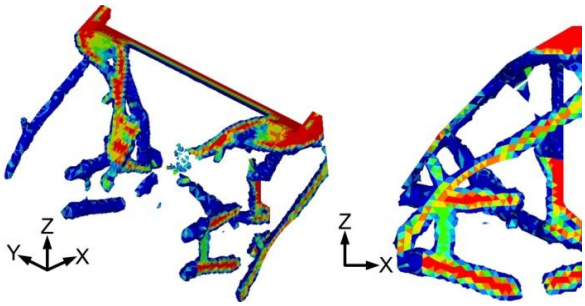

Fig. 9: Front topology

Fig. 9 illustrates a well defined topology which, as previously mentioned, is a general tendency for all models, with only minor (local) changes of topology between different models. These local variations were, in general, located in the vicinity of where the CBC models were constrained. A general tendency for the rear area topology also existed. This tendency, illustrated in Fig. 10, was also distinguishable across models, regardless of BC type.

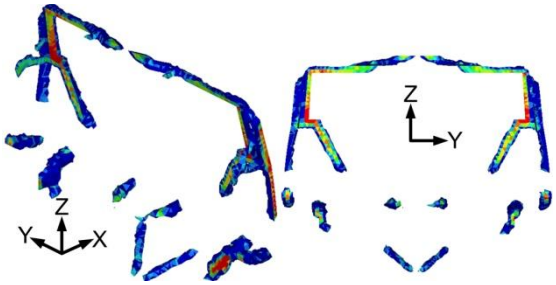

Fig. 10: Rear topology

Fig. 10 displays a well defined topology, which (coupled with the fact that it is a general tendency) indicates that the results illustrated in Fig. 10 represent a "converged" topology for the rear area. The results of the topology optimisations discussed so far have only displayed minor (localised) changes of topology within the specific areas in question. These changes were caused by change of CM locations and/ or a change in selected BC. The topology of the final area to be discussed is the floor, as indicated in Fig. 6. The changes of topology of this area were significantly more substantial, with respect to a change of BC. Therefore, at this point it was necessary to once again group the models by BC type, starting with the CBC models. In line with the previously discussed results these models showed a general tendency which was applicable to all CBC models. Only very minor local changes of topology were found, when the location of CM was altered. The generalised topology is illustrated in Fig. 11.

A similar tendency did not exist within the IR models; in fact the IR models did not display a general trend, as shall be discussed later. Fig. 12 illustrates the topology obtained by the IR model corresponding to the CBC model illustrated in Fig. 11 (which is model 49). An appreciation of the difference in results obtained by CBC and IR models can thus initially be understood by comparing Fig. 11 to Fig. 12. Throughout this Section, and culminating with Fig. 11, it has been underlined that the effects of the location of CM upon the resulting topology were localised, with respect to the CBC models. This statement essentially summarises the outcome of the topology optimisation study, with respect to the CBC models; namely that the location of the battery pack and range extender / fuel tank within the BIW had a trivial influence upon the topology optimisation results. Based upon the above, the number of possible responses to the ultimate aim of this study, which was to find the optimal locations of these components within the BIW with respect to reducing BIW mass, is simply infinite. So why did the resulting BIW topology not change significantly with the location of the CM for the CBC models? A likely answer was simply the magnitude of the forces involved in each load case.

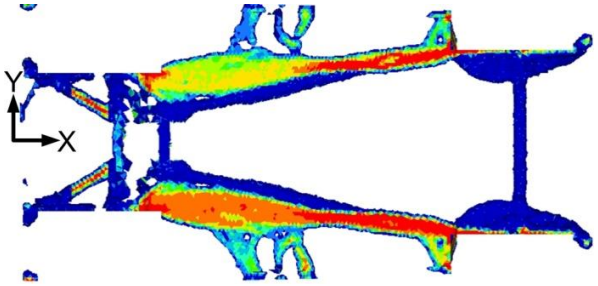

Fig. 11: Floor topology, CBC

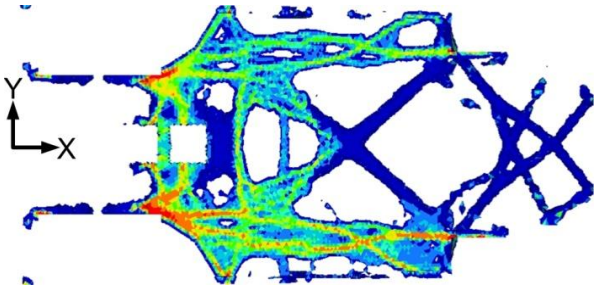

Fig. 12: Floor topology, IR

The highest magnitude forces are found in the front crash (ODB) and the high speed rear impact load cases, as defined in Section 1.2. Comparing these to the magnitude of the forces originating from inertial effects of the components the difference was 90%.This relationship was repeated throughout the individual load cases, i.e. the force magnitude originating from component mass was significantly less than that of the associated "external" force. Therefore it was thought that the optimisation for the CBC models was primarily dictated by the external forces, drastically reducing the influence of the forces originating from component mass. Substantiation of the above statement was sought by studying the results of model 73, wherein the component mass value was scaled by a factor of 2, as specified in Section 3.1. However, the results of this model did not indicate any significant changes relative to the remaining CBC models. In a final attempt to investigate the correctness of the above statements, the aforementioned 74th CBC model was introduced. In this model the mass values were scaled by a factor of 3 (from the original, not model 73), despite this increase no significant differences were found. However, with this model, the forces in question were still only approximately 1/3 the magnitude of the "external" forces. At this point it could be argued to further increase the "mass scaling" however the relevance of such a model could be seriously questioned.

Returning to Eqn. (2), model 73 represents a battery pack with a mass of 300 kg exposed to a deceleration of 30gand a range extender / fuel tank of 220kg exposed to 30g. The relevance of increasing these values with respect to achieving the overall aim was questionable at best. Therefore, no specific (optimal) location of the battery pack nor range extender / fuel tank within the BIW could be found by means of the CBC models. With the above in mind, the focus turned to the floor topology of the IR models. These results clearly showed significant differences between models, when the locations of CM were altered. These differences were also reflected when the mass reduction (in %) of the individual models was calculated, using Eqn. (5).

$$\text{Mass reduction} = 100 - \left(\frac{\text{FIMV}}{\text{ZIMV}}\right)\cdot 100 \qquad (5)$$

Where FIMV is the mass value of the final iteration, and ZIMV is the mass value of the initial (0th) iteration. The above thus meant that the performance of the individual models, with respect to achieving the ultimate aim of the study, could now be specifically evaluated on a model by model basis. This was also the case with the CBC models, but the significant difference was that with the IR models the individual models stand out by displaying variety in floor topology and even more importantly in the value of mass reduction. The scope of mass reduction value for the 73 IR models ranged from approximately 81.2% to 91.2%. The corresponding range for the CBC models was 88.0% to 90.1%, thereby underlining the significant difference in results obtained.

Comparing the average mass reduction values of the CBC and IR models also revealed an interesting fact, namely that the average mass reduction values of the IR models was greater than those of the CBC models. The average mass reduction value of the IR models was 89.5% compared to 88.9% for the CBC models. Primarily based upon the above findings, nine models were selected for further investigation. The selection criteria for these nine models, which were all IR models, was that they all showed a mass reduction in excess of 90.0%.These models are all listed in Table 2.

The general setup of models 65, 68, and 72 are slightly different relative to that of the remaining models listed in Table 2. To summarise these differences model 65 had a larger "battery area" in the xy-plane (Fig. 6) than the others, this covered the areas denoted in Table 2 and illustrated in Fig. 6. Model 68 contained a coincident location for both components, i.e. a mass value of 260 kg

was located at point 14, Fig. 4. Finally, model 72 did not contain any mass for the components, and thus represented the BIW without the influence of the battery pack and range extender / fuel tank. Unsurprisingly model 72 (which essentially is a replica of model 69) represented the largest mass reduction value, undoubtedly due to the absence of the component masses. Model 72 was therefore used as a bench mark to evaluate the remaining models, simply because it was unaffected by the components, i.e. the influence upon topology of the additional mass from the components was eliminated.

Table 2: Models selected

Model # (IR)	CM (battery pack)	CM (RE / FT)	Mass red.
19	16	15	90.0%
34	14	13	90.2%
35	15	13	90.3%
42	15	14	90.0%
43	16	14	90.1%
49	16	15	90.0%
65	1,7,16,25,31	20	90.0%
68	14	14	90.0%
72	N/A	N/A	91.2%

Comparing the 91.2% reduction of model 72 to the average mass reduction value of the remaining models listed in Table 2 it was found that the difference was approximately 1.1%, which was deemed insignificant compared to the additional 260 kg of mass included in these models. Another interesting fact, which can be found by studying Table 2 is the fact that all models listed (with the exception of model 72) have located the CM of all components in the symmetry line (i.e. the x-axis) of Fig. 6. At this point the 73 initial models have been reduced to nine including model 72, which was not a viable solution. The next step was therefore to investigate the sensitivity of the remaining models.

3.3. IR models sensitivity study

The purpose of this study was to determine the sensitivity of the models listed in Table 2, with respect to certain variations. The study was divided into three major parts:

- Angle sensitivity.
- Stiffness sensitivity.
- Combined angle and stiffness sensitivity.

The angle sensitivity study was performed by including additional load cases within the specific models. These load cases were replicas of the front crash (ODB) and the high speed rear impact load cases. Please note that the original load cases as defined in Section 1.2 were still applied. Neither the application points nor the force magnitudes were altered during this study, only the angles. Fig. 13 illustrates these angles.

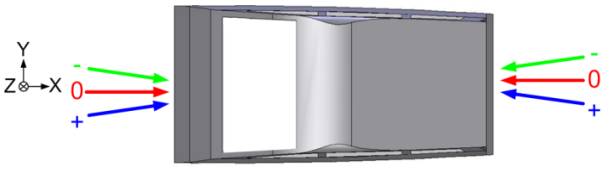

Fig. 13: Load angles

The "0" arrows in Fig. 13 represents the "original" load cases, i.e. the ones defined in Section 1.2. The additional load cases contained separate plus and minus load cases. This was carried out for 5˚ and 10˚ angles, in addition to a combination of the two. This led to a total of 4 different variations of each of the single models listed in Table 2, specified as:

1. Original model (i.e. no additional load cases)
2. 5˚ load case additions:
   a. 5˚ + front crash (ODB)
   b. 5˚ - front crash (ODB)
   c. 5˚ + high speed rear impact
   d. 5˚ - high speed rear impact
3. As specified in point 2 above, but with 10˚ angles.
4. Both 5˚ (point 2) and 10˚ (point 3) load case additions.

The permutations above created an additional (9 x 3) 27 models. The results from these additional models showed a further change in (particularly) the floor area between the "original models" (point 1) and the models with additional load cases (points 2-4). However, the individual differences between the latter models, i.e. points 2-4 above, were not found to be significant. An example of the above differences can be seen in Fig. 14, which represents the results of the angle sensitivity study of model 19, also including parts of the front area and rear area topology. The upper illustration in Fig. 14 represents the original model, while the lower illustration represents the general topology of the remaining three models, as the individual differences between these three was not found to vary significantly.

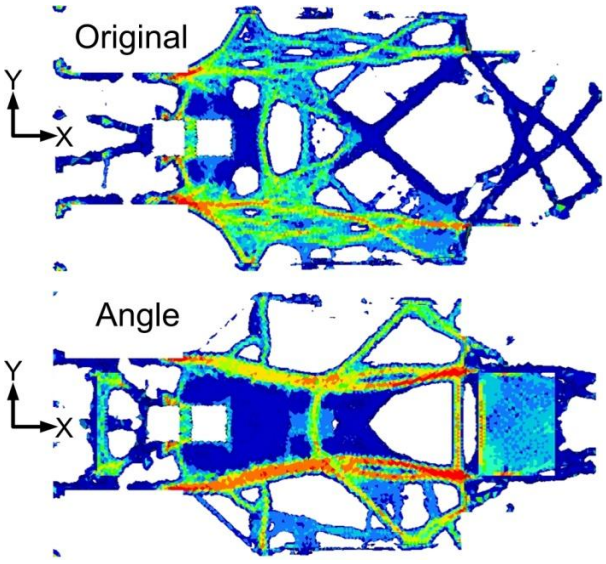

Fig. 14: Floor topology, angle sensitivity study

The differences between the two illustrations in Fig. 14 are clear, underlining the sensitivity of the models with respect to the angle of application for these particular load cases. In other words, a difference was found between models including point 1 above (upper illustration in Fig. 14), and any combination of points 2-4 above (lower illustration in Fig. 14). The individual differences between models including the load cases of points 2-4 above, did not display any significant differences, and are thus all represented by the lower

illustration in Fig. 14. This tendency was also found for the remaining models listed in Table 2. These results thus also substantiate the previous statement that the topology optimisation was primarily dictated by the (largest) external forces.

The next step in the IR models sensitivity study was the stiffness study. The basis of this study was the original models listed in Table 2, i.e. the additional load cases of the angle study were omitted from this study. The implementation of the battery pack and range extender / fuel tank within the actual models consisted of excluding specific elements from the design domain, while adding the required concentrated nodal masses. These elements were solid elements with linear displacement functions, and the material characteristics of mild grade steel, as defined in Sections 1.2 and1.4. This was the equivalent of having a "solid" steel plate in these locations, including the associated stiffness. Thereby, it was assumed that the performance of the components, e.g. the battery pack, during loading was equivalent to the performance of the aforementioned steel plate, which was a significant performance requirement. The reasoning behind this was that if these components were part of the main load bearing structure (i.e. the crash structure) then no additional or unnecessary mass would be added in order to attach the components to the BIW.

A counter argument to the above could be made by firstly questioning whether it was at all possible to achieve the required performance of the components in question, and secondly, should this performance be achieved, how did this influence the manufacturing and material cost in addition to the mass of e.g. the battery pack (or perhaps more appropriately the battery box). In addition the question could be raised as to how much (if any) mass would be added to the BIW if the performance of the components is lowered and whether this value would be in excess of the expected gain in mass of e.g. the battery pack. The above questions can not all be answered at this point in time, simply because of their complexity.

However, a first step in the effort to answer these was taken by means of this stiffness study; namely how much mass will be added to the models, if the battery pack compliance was lowered. In order to achieve this, the stiffness value (i.e. Young's Modulus) of the component areas was altered. This was done in 4 different steps (per model listed in Table 2), these being:

- 210 GPa (original)
- 70 GPa
- 35 GPa
- 17.5 GPa

This also leads to an additional 27 models, as was the case with the angle study. The general outcome of this study was that the influence of the stiffness upon the topology optimisation results was minimal. However, at this point it must be underlined that the areas in question were (generally) 250 mm by 250 mm, as defined in Section 1.3, making them small compared to the overall dimensions of the design volume. This obviously had an effect on the results of the study. The exception of the above is model 65 which utilised a considerably larger area to represent the battery pack. The results of this model are illustrated in Fig. 15, where the areas marked with an x represent the size of the battery pack. Please note, that Fig. 15 also includes parts of the front and rear area topology.

Fig. 15 clearly shows a significant difference with respect to the floor topology, which was not found in the remaining models in the stiffness sensitivity study. This was, as previously mentioned, not unexpected as the area with the reduced stiffness was significantly larger in model 68 when compared to the remaining models listed in Table 2. The topology illustrated in the lower part of Fig. 15 contains a less distinctive/defined topology than the upper illustration in Fig. 15, which could possibly be resolved by adjusting the penalisation factor p. However, to fully understand the implications of the reduced stiffness value the global topology was reviewed, because the changes were no longer localised to the floor area, although the most significant differences were still found there. An interesting fact was that the mass reduction of the 210 GPa model was exactly the same as the 17.5 GPa model, namely 90.0%. The above indicated that when the "external" forces, i.e. the ones defined in Section 1.2 were applied the distribution of these throughout the BIW had changed (between e.g. the 210 GPa and the 17.5 GPa) model, which was also substantiated by the global change of topology. It had been established that both the angle and the stiffness significantly influence the outcome of the topology optimisation; therefore these must be taken into account.

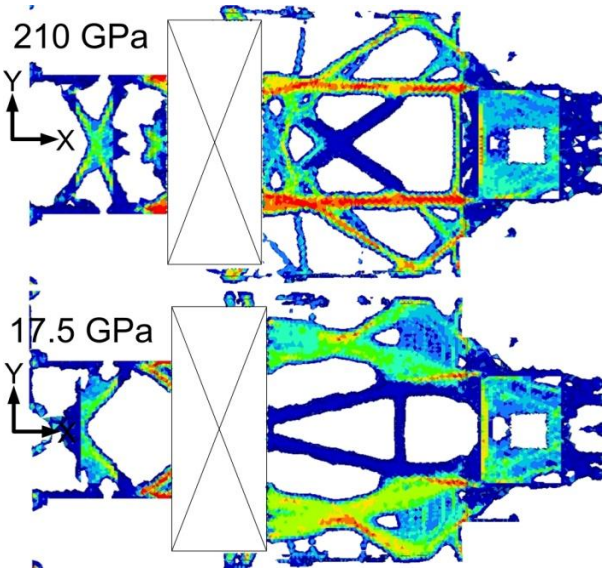

Fig. 15: Floor topology, stiffness sensitivity study

The next step was therefore to conduct a combined study incorporating both angles and stiffness in one study, this produced a total of 144 models (in addition to the original CBC / IR study). The results and implications of this study exceed the scope of this paper, however an important (and general trend) was identified. This trend was identified by observing the individual models' mass reduction value as a function of the associated angles and stiffness values, based upon model 65. The trend found was simply that the mass reduction value did not vary significantly with the combined angle and stiffness variations, thus indicating that changing

these parameters did not influence the topology optimisation results, i.e. mass reduction values. However, the combined angle and stiffness study did identify a significant change in the global topology, such as the one illustrated in Fig. 15. In general it was found that if the stiffness of the battery pack was lowered, the relative element density of the floor area would decrease, while it would increase for the roof area. The next and final Sections of this paper discuss the general results found, the lessons learnt and the suitability of the methodology used, in addition to the possible next steps.

3.4. Discussion of topology results

The general findings presented in this paper will now be summarised with respect to the individual areas defined by Fig. 6. The generalised topology of the roof area has remained very consistent throughout the entire study, while utilising both CBC and IR, and also including the sensitivity studies, wherein only minor changes occurred. The simple conclusion is that the topology of this area has converged. This converged topology was, as previously mentioned, unconventional when compared to the roof bow structures of many modern day passenger vehicles. The side area topology has, in line with the roof topology, also remained consistent, however, a significant number of the models display a rather vague definition of the side area topology, as illustrated by Fig. 8. Therefore additional optimisation studies will be required in order to achieve a more refined topology for this area. The floor area topology was found to produce the most significant changes in topology during the studies. The implications of the battery pack and range extender / fuel tank CM were used to isolate 9 models whereof 8 are potential solutions to location of these CM.

The effects of angles and stiffness upon the floor topology were investigated, leading to a suspected link between component (e.g. battery pack) compliance and BIW mass. In general the individual floor area topologies were found to be viable solutions that can be implemented in order to successfully withstand the dynamic crash loading scenarios. However this is solely based upon mechanical engineering judgements and is not at this point backed up by any calculations. The results relating to the roof, floor and partially the side area topologies, which in essence make up the safety cage of the vehicle, generally display relatively well defined load paths. The front and the rear areas were also found to change significantly with angles and stiffness values, as indicated in Fig. 14 and in Fig. 15.

The response of the topology optimisation with respect to the front and rear areas, primarily as a function of changing the angles, seems to be “triangulation”, i.e. the widespread use of triangles. This makes perfect sense from a linear static point of view, as the stiffest geometry in solid mechanics is indeed a triangle. However, this raises serious concerns when the subsequent step is taken into dynamic loading, primarily because of the triangles resistance to buckling, which undoubtedly will have a negative influence on the crushability, and therefore the dynamic crash performance of these very vital areas. This is evidently one of the major limitations of the linear solver and highlights the necessity for further steps in the optimisation procedure.

4. Conclusion and Further Work

The discussions and the results presented throughout this paper have led to the definition of an alternative approach to BIW design. The results and methodology presented are only the initial steps. However, it demonstrates the efficiency of this technique, whilst underlining the valuable outcomes which can be implemented in the continued BIW development process. These outcomes primarily determine the outline requirements for structural load path development and mass distribution. These were obtained by relatively simple modelling techniques, nevertheless implementing the required complexity in order to create a good starting point for the continued BIW design process. An example of this is illustrated in Fig. 16.

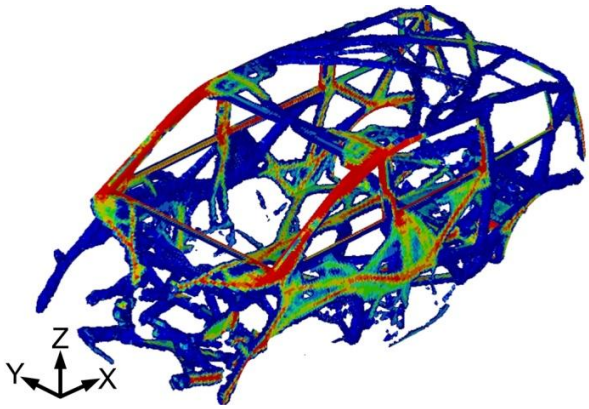

Fig. 16: Iso metric view, IR topology optimisation example

However, as discussed, there are some limitations of the linear (or implicit) topology optimisation. This method cannot fully consider inertial effects as well as other aspects such as detailed material property characteristics, strain rate effects, real world effects such as the interaction of the vehicle to its surroundings (ground and barrier) and also the interaction of the assemblies within the vehicle it-self cannot be included. The particular topology optimisation process presented in this paper also utilises simplified panel joining methodology in addition to the joining of sub-assemblies. To enhance the output of the linear topology optimisation, an explicit optimisation process could be developed, such as discussed in [7]. This process will likely use explicit crash analysis modelling techniques, in order to generate a finite element representation of the linear structure, and subject it to (dynamic) crash loading. However, this step is likely to be very extensive, and before commencing, the choice of methodology should be painstakingly considered, such as discussed in [8], [9], [10], [11] and [12].

This process should include development of material properties where practicable, in addition to including relevant and available vehicle sub-assemblies [13], [14]. The intention is that this process will optimise the shape and material properties of the crash structure in order to provide a suitable structure for high speed dynamic crash impact.

ACKNOWLEDGEMENTS:

The authors of this paper would like to thank Mike Dickison, Richard Nicholson (both of Coventry University), Tata Motors European Technical Centre (TMETC), Jaguar Land Rover (JLR), Warwick Manufacturing Group (WMG) and other contributors to the Low Carbon Vehicle Technology Project (LCVTP) for supplying data and guidance to assist in the making of this paper.

REFERENCES:

[1] N. Jones. 2001. Dynamic material properties and inelastic failure in structural crashworthiness, *Int. J. Crashworthiness*, 6(1), 7-18. doi:10.1533/cras.2001.0158

[2] C.B.W. Pedersen. 2003. Topology optimization for crashworthiness of frame structures, *Int. J. Crashworthiness*, 8(1), 29-39. doi:10.1533/ijcr.2003.0218

[3] C. Bastien, J. Christensen, M. Dickison, A. Gittens, R. Nicholson , and O. Tomlin. 2010. Topology optimisation of a body in white for low carbon vehicle technology project, *European HyperWorks Technology Conf*., Versailles, France.

[4] A.R. Barnett and T.W. Widrick. 2005. *Closed-Form Static Analysis With Inertia Relief and Displacement-Dependent Loads Using a MSC/NASTRAN DMAP Alter*, NASA Tech. Report 19950013233_1995113233.

[5] *Altair Hyperworks Manual*, 2010, Altair Engg. Inc., Troy, Michigan, USA.

[6] P.R. Marur and S. Srinivas. 2008. A reduced-order finite element model for the simulation of automotive side structure crash response, *Int. J. Crashworthiness*, 13(2), 211-218.

[7] C.A. Soto. 2004. Structural topology optimization for crashworthiness, *Int. J. Crashworthiness*, 9(3), 277-283. doi:10.1533/ijcr.2004.0288

[8] F. Duddeck. 2007. *Multidisciplinary Optimization of Car Bodies*, Springer Publications, London, UK.

[9] H. Zimmer, M.Prabhuwaingankar and F. Duddeck. 2009. Topology & geometry based structure optimization using implicit parametric models and LS-OPT, *Proc. 7th European LS-Dyna Conf.*, Salzburg, Austria.

[10] E. Acar and K. Solanki. 2009. Improving the accuracy of vehicle crashworthiness response predictions using an ensemble of metamodels, *Int. J. Crashworthiness*, 14(1), 49-61. doi:10.1080/13588260802462419

[11] X. Liao, Q. Li, X. Yang, W. Li and W Zhang. 2008. A two-stage multi-objective optimisation of vehicle crashworthiness under frontal impact, *Int. J. Crashworthiness*, 13(3), 279-288. doi:10.1080/13588260801933659

[12] M.F. Horstmeyer, X.C. Ren, H. Fang, E. Acar and P.T. Wang. 2009. A comparative study of design optimisation methodologies for side-impact crashworthiness, using injury-based versus energy-based criterion, *Int. J. Crashworthiness*, 14(2), 125-138. doi:1s0.1080/13588260802539489

[13] *LS-Dyna Users Manual*, 2010, Livermore Software Technology Corporation, California, USA.

[14] P.A. Du Bois. 2004. *Crashworthiness Engineering Course Notes*, Livermore Software Technology Corporation, California, USA.